Influence of the Rice Factor on the Performance of Blind Detectors for Cooperative Spectrum Sensing

Dayan A. Guimarães and Luiz G. B. Guedes

***Abstract*— Most spectrum sensing research relies on simple sensing channel models like pure Gaussian or Gaussian with fading, normally Rice or Rayleigh. Often, a fixed Rice factor is assumed across the coverage area, disregarding variable line-of-sight conditions between primary and secondary users. However, the Rice factor is an environment-dependent random parameter, and this study examines its impact on the performance of state-of-the-art blind detectors for cooperative spectrum sensing. It also takes into account other realistic scenarios like distance-dependent signal powers, nonuniform receiver noise, and consistent signal-to-noise ratio calibration. Findings reveal significant effects on certain detectors, with some showing resilience to Rice factor fluctuations.**

***Keywords*— Cognitive radio, dynamic spectrum access, Rice factor, spectrum sensing.**

I. Introduction

The proliferation of wireless communication systems in recent years has led to the radio frequency (RF) spectrum becoming a scarce resource, attributed to the adoption of fixed spectrum allocation policies, wherein a network of primary users (PUs) holds exclusive rights to use a certain RF band. However, studies indicate that many allocated RF bands remain underutilized in certain regions and periods, leading to inefficient spectrum usage [1], [2].

The scenario of RF spectrum scarcity is expected to worsen, for instance due to the expansion of both Internet of things (IoT) and 5G networks and the realization of the 6G networks, which will require larger bandwidths and intensify the contention for the already limited spectrum [1]–[3].

A potential solution to the problem of inefficient spectrum usage is the adoption of cognitive radio (CR) networks, where vacant bands resulting from the variable occupancy of the primary network spectrum in time and space can be identified [4]. In this case, a dynamic spectrum access (DSA) policy can be adopted, wherein cognitive terminals of secondary users (SUs) opportunistically use unoccupied frequency bands. The so-called spectrum sensing, with or without the assistance of a database of RF spectrum occupancy, is the technique used by the secondary network to detect spectral gaps, also known as whitespaces or spectrum holes [2], [3], [5]–[7].

Dayan A. Guimarães and Luiz G. B. Guedes are with the National Institute of Telecommunications (Inatel), Santa Rita do Sapucaí, MG, Brazil, e-mail: dayan@inatel.br; luiz.guedes@mtel.inatel.br. This work was partially supported by RNP with resources from MCTIC Grant 01245.020548/2021-07 under the 'Brazil 6G Project' of the Radio-communication Reference Center of Inatel; by EMBRAPII-Inatel Competence Center on 5G and 6G Networks with resources from PPE-00124-23 of FAPEMIG and PPI IoT/Manufacture 4.0 of MCTI under the project 'XGM-AFCCT-2024-4-1-2' Grant 052/2023; by FAPESP Grant 2022/09319-9; and by CNPq Grant 302589/2021-0.

While individual spectrum sensing by each SU may be compromised by multi-path fading, signal shadowing, and hidden terminals, cooperative spectrum sensing (CSS) involves multiple SUs to improve the accuracy of decisions regarding the occupancy state of the sensed band [7].

In this article, a centralized CSS with data fusion is considered. The samples of the signal received by the SUs are transmitted to the fusion center (FC) for the calculation of a test statistic and its comparison with a decision threshold, aiming to reach a global decision regarding the occupancy state of the monitored band.

Among the various detectors for spectrum sensing proposed in the literature, this work considers state-of-the-art blind detectors, which do not make use of any information about the detected signal or the noise variance, namely: the Gerschgorin radii and centers ratio (GRCR) detector [8], the Gini index detector (GID) [9], the Pietra-Ricci index detector (PRIDe) [10], the Hadamard ratio (HR) detector [11], the volume-based detector number 1 (VD1) [12], the generalized likelihood ratio test (GLRT) based on eigenvalues [13], the maximum-minimum eigenvalue detector (MMED) [13], the arithmetic to geometric mean (AGM) detector [14], and a detector based on the locally most powerful invariant test (LMPIT) [15].

The computational burden required to form the test statistics of such detectors varies depending on the necessary operations: the HR and VD1 primarily depend on calculating the determinant of the received signal sample covariance matrix (SCM). The detectors AGM, MMED, and GLRT make use of estimates of the eigenvalues of this matrix. On the other hand, the GID, GRCR, PRIDe and LMPIT operate directly on the elements of the SCM, being particularly noteworthy for having lower computational complexity and being more robust against variations in signal power and noise than the other above-mentioned detectors. Among these, the PRIDe has the lowest complexity, closely followed by the GID, GRCR and LMPIT [8]–[10], [15].

As far as the model for the PU-to-SUs channel is concerned, the majority of research on spectrum sensing adopt the simple additive white Gaussian noise (AWGN) model, or the AWGN plus signal fading models, especially the Rice, or its particular case of Rayleigh fading. The Rice factor (or Rice K-factor) is the ratio between the signal strength received via a dominant propagation path, for example in a line-of-sight (LoS) condition or specular reflection, and the power contained in the signals from the other paths. A larger Rice factor means less variability in the instantaneous received signal strength. A null Rice factor means the absence of a dominant path, which corresponds to a Rayleigh fading. In practice, a Rice factor

greater than 10 corresponds to a channel approximately free of fading [7].

When the Rice fading is adopted, it is also common that the Rice factor is kept fixed and the same for the entire coverage area. However, it is not reasonable to adopt such assumption, since the line-of-sight conditions between the PU transmitter and the SUs differ from place to place. This is evidenced by the results presented in [16], where the Rice factor is shown to be an environment-dependent random variable. Aligned with this fact, this paper assesses the influence of the Rice factor on the performance of the previously-described state-of-the-art detectors. Complementing this contribution, the paper also adopts other realistic assumptions about the system model, such as distance-dependent received signal powers, nonuniform noise levels among the SUs' receivers, and a consistent process for calibrating the signal-to-noise ratio (SNR).

The remainder of this article is organized as follows. Section II describes the models for signals, noise and channel. The test statistics of the detectors listed in this section are presented in Section III. Section IV is devoted to numerical results and discussions, with Section V concluding the work.

II. Signal, noise and channel models

The model for centralized CSS with data fusion adopted herein is based on [9], [10], but with important improvements in the computation of the SNR and in the way of determining the powers of the received signals at the SUs, likewise in [17] and [18]. Spectrum sensing is performed by m cooperating SUs, each collecting n samples of the primary signal during a sensing interval. The collected samples are transmitted to the FC through an error-free control channel, forming the sample matrix $\mathbf{Y} \in \mathbb{C}^{m\times n}$, which is given by

$$\mathbf{Y} = \mathbf{h}\mathbf{x}^{\mathrm{T}} + \mathbf{V}, \tag{1}$$

where the vector $\mathbf{x} \in \mathbb{C}^{n\times 1}$ contains the samples of the primary signal, which are modeled as complex Gaussian random variables with zero mean, which relates to modeling modulated signal envelope fluctuations. The channel vector $\mathbf{h} \in \mathbb{C}^{m\times 1}$ is formed by elements h_i representing the channel gains between the PU transmitter and the ith SU, for $i = 1, \ldots, m$. The variation of these gains over time models the fading effect produced in the signal due to multi-path propagation and the mobility of the SUs. It is defined that $\mathbf{h} = \mathbf{G}\mathbf{a}$, where $\mathbf{G}$ is a gain matrix to be defined later, and $\mathbf{a} \in \mathbb{C}^{m\times 1}$ is a vector formed by complex Gaussian random variables $a_i \sim \mathbb{C}\mathcal{N}[\sqrt{K/(2K+2)}, 1/(K+1)]$, with $K = 10^{K^{(\mathrm{dB})}/10}$ being the Rice factor of the channels between PU and SUs, and $K^{(\mathrm{dB})} = 10\log_{10}(K)$ in dB.

Based on measurements reported in [16], it was concluded that $K^{(\mathrm{dB})}$ is a random variable that can be well characterized by a Gaussian distribution with mean μ_K and standard deviation σ_K, both in dB, i.e., $K^{(\mathrm{dB})} \sim \mathcal{N}[\mu_K, \sigma_K]$. Typical values of μ_K and σ_K are determined according to the propagation characteristics imposed by the environment [16]. For example, in urban areas, typically $\mu_K = 1.88$ dB and $\sigma_K = 4.13$ dB. In rural or open areas, $\mu_K = 2.63$ dB and $\sigma_K = 3.82$ dB. Suburban regions are commonly associated with $\mu_K = 2.41$ dB and $\sigma_K = 3.84$ dB [16].

The present modeling also allows for the received signal power levels at the SUs to be unequal and time-varying due to the different distances between the PU transmitter and the SUs, as well as due to the variation of these distances in different sensing events caused by the movement of the SUs. In this case, the previously mentioned gain matrix $\mathbf{G} \in \mathbb{R}^{m\times m}$ is given by $\mathbf{G} = \mathrm{diag}(\sqrt{\mathbf{p}/P_{\mathrm{tx}}})$, where $\mathbf{p} = [P_{\mathrm{rx}1}, \ldots P_{\mathrm{rx}m}]^{\mathrm{T}}$ is the vector of PU signal powers received by the m SUs, with $[\cdot]^{\mathrm{T}}$ denoting transposition. P_{tx} is the PU's transmission power in watts, and $\mathrm{diag}(\cdot)$ returns a diagonal matrix whose diagonal is formed by the elements of the vector in the argument.

The log-distance path loss prediction model [19] is utilized here to calculate the received signal power by the ith SU, in watts, as given by

$$P_{\mathrm{rx}i} = P_{\mathrm{tx}}\left(\frac{d_0}{d_i}\right)^{\eta}, \tag{2}$$

where d_0 is a reference distance in the far-field region of the transmitting antenna, d_i is the distance between the PU and the ith SU, and η is the path loss exponent. All distances are given in meters.

Differences and variations in noise powers at the SUs' receivers may occur due to temperature variations, differences between the front-ends, and undesired signals entering the receivers and acting as noise [17]. To model such condition, the elements of the ith row of the matrix $\mathbf{V} \in \mathbb{C}^{m\times n}$ given in (1) are zero-mean Gaussian random variables with variance

$$\sigma_i^2 = (1 + \rho u_i)\bar{\sigma}^2, \tag{3}$$

where u_i is a realization of a uniform random variable U_i in the interval $[-1, 1]$, $\bar{\sigma}^2$ is the average noise power at the SUs, and $0 \leq \rho < 1$ is the fraction of variation of the noise power σ_i^2 around $\bar{\sigma}^2$.

The instantaneous signal-to-noise ratio at the SUs, γ, is a random variable because it depends on σ_i^2 and d_i, which are random. In light of (2) and (3), a realization of γ is given by

$$\gamma = \frac{1}{m}\sum\nolimits_{i=1}^{m} \frac{P_{\mathrm{tx}}\,(d_0/d_i)^{\eta}}{(1+\rho u_i)\bar{\sigma}^2}. \tag{4}$$

Thus, the average SNR of the SUs is given by $\mathrm{SNR} = \mathbb{E}[\gamma]$, where $\mathbb{E}[\gamma]$ is the expected value of γ. To realize this SNR model, it is firstly calculated the expected value of γ', defined for $\bar{\sigma}^2 = 1$ and $\{d_i\}$. It can be shown [17] that it is given by

$$\mathbb{E}[\gamma'] = \ln\left(\frac{1+\rho}{1-\rho}\right)\frac{1}{2\rho m}\sum\nolimits_{i=1}^{m} P_{\mathrm{rx}i} \tag{5}$$

for $0 < \rho < 1$, and for $\rho = 0$ it is given by

$$\mathbb{E}[\gamma'] = \frac{1}{m}\sum\nolimits_{i=1}^{m} P_{\mathrm{rx}i}. \tag{6}$$

As $\mathrm{SNR} = \mathbb{E}[\gamma] = \mathbb{E}[\gamma']/\bar{\sigma}^2$, the calibrated noise power becomes

$$\bar{\sigma}^2 = \frac{\mathbb{E}[\gamma']}{\mathrm{SNR}}. \tag{7}$$

This value of $\bar{\sigma}^2$ is then plugged into (3), along with a realization u_i of the random variable U_i, to determine σ_i^2, the variance of the noise samples in the ith row of $\mathbf{V}$. New values of $\{\sigma_i^2\}$ are calculated for each sensing event, providing temporal variability to the noise levels.

The matrix $\mathbf{Y}$ defined in (1) is formed at the FC from the mn samples sent by the SUs. Under hypothesis $\mathcal{H}_1$, the primary signal is present in the sensed band, i.e., $\mathbf{Y} = \mathbf{h}\mathbf{x}^{\mathrm{T}} + \mathbf{V}$. Under hypothesis $\mathcal{H}_0$, the primary signal is absent, leading to $\mathbf{Y} = \mathbf{V}$.

III. Detectors' test statistics

All detectors presented in this section make use of the received signal sample covariance matrix (SCM) of order $m \times m$, which is computed at the FC and is given by

$$\mathbf{R} = \tfrac{1}{n}\mathbf{Y}\mathbf{Y}^{\dagger}, \tag{8}$$

where $\dagger$ denotes conjugate transposition.

The test statistic of the GRCR detector [8] is given by

$$T_{\text{GRCR}} = \frac{\sum_{i=1}^{m}\sum_{j=1, j\neq i}^{m} |r_{ij}|}{\sum_{i=1}^{m} r_{ii}}, \tag{9}$$

where r_{ij} is the element on the ith row and jth column of $\mathbf{R}$.

The GID [9], [17] and PRIDe [10], [20] test statistics are respectively computed according to

$$T_{\text{GID}} = \frac{\sum_{i=1}^{m^2} |r_i|}{\sum_{i=1}^{m^2}\sum_{j=1}^{m^2} |r_i - r_j|}, \tag{10}$$

$$T_{\text{PRIDe}} = \frac{\sum_{i=1}^{m^2} |r_i|}{\sum_{i=1}^{m^2} |r_i - \bar{r}|}, \tag{11}$$

where r_i, for $i = 1, 2, \ldots, m^2$, is the ith element of the vector $\mathbf{r}$ formed by stacking all columns of $\mathbf{R}$, and $\bar{r} = (1/m^2)\sum_{i=1}^{m^2} r_i$.

The HR test statistic [11] is given by

$$T_{\text{HR}} = \frac{\det(\mathbf{R})}{\prod_{i=1}^{m} r_{i,i}}, \tag{12}$$

where $\det(\mathbf{R})$ is the determinant of $\mathbf{R}$.

The VD1 detector [12] has a test statistic given by

$$T_{\text{VD1}} = \log\left[\det(\mathbf{E}^{-1}\mathbf{R})\right], \tag{13}$$

where $\mathbf{E} = \text{diag}(\mathbf{e})$, with $\text{diag}(\mathbf{e})$ being the diagonal matrix whose main diagonal corresponds to the vector $\mathbf{e} = [e_1, e_2, \ldots, e_m]$, where $e_i = \|\mathbf{R}(i,:)\|_2$ and $\|\cdot\|_2$ denotes the Euclidean norm.

The test statistics of the eigenvalue-based detectors GLRT [13], MMED [13] and AGM [14] are respectively computed according to

$$T_{\text{GLRT}} = \frac{\lambda_1}{\frac{1}{m}\sum_{i=1}^{m}\lambda_i}, \tag{14}$$

$$T_{\text{MMED}} = \frac{\lambda_1}{\lambda_m}, \tag{15}$$

$$T_{\text{AGM}} = \frac{\frac{1}{m}\sum_{i=1}^{m}\lambda_i}{\left(\prod_{i=1}^{m}\lambda_i\right)^{1/m}}, \tag{16}$$

where $\{\lambda_1 > \lambda_2 > \cdots > \lambda_m\}$ are the eigenvalues of $\mathbf{R}$.

In the case of the LMPIT detector [15], the test statistic is

$$T_{\text{LMPIT}} = \sum_{i=1}^{m}\sum_{j=1}^{m} |c_{ij}|^2, \tag{17}$$

where c_{ij} is the element on the ith row and jth column of the matrix $\mathbf{C} = \mathbf{D}^{-1/2}\mathbf{R}\mathbf{D}^{-1/2}$, for $i, j = 1, 2, \ldots, m$, where $\mathbf{D}$ is the diagonal matrix whose diagonal elements are $d_{ii} = r_{ii}$.

The decision regarding the occupancy state of the sensed band is made by comparing any of the test statistics above with a predefined decision threshold θ, according to the desired false alarm rate. In practice, this threshold is determined in the system design phase. If $T > \theta$, the decision is made in favor of $\mathcal{H}_1$. Otherwise, $\mathcal{H}_0$ is chosen.

IV. Numerical results

The cooperative spectrum sensing topology adopted in this paper is exemplified in Fig. 1. It comprises a secondary network with m SUs ($m = 10$ in this figure) that are uniformly distributed in a circular coverage area with radius r meters. A normalized $r = 1$ has been used in Fig. 1, with the PU transmitter located at $(x, y) = (1, 1)$ meters. The FC, which can be the base station of the secondary network, is located at the center of the coverage area. In each sensing event, new random positions of the SUs are determined, aiming at simulating mobile SUs.

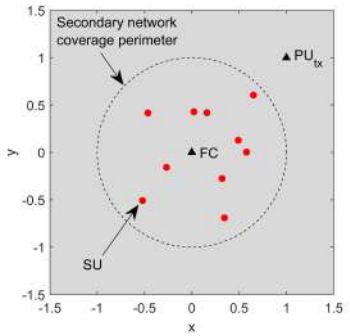

Fig. 1: CSS topology for $m = 10$ SUs, normalized coverage radius $r = 1$ m, FC at $(x, y) = (0, 0)$, and PU transmitter at $(x, y) = (1, 1)$.

The range of values of the Rice K-factor considered herein is from -10 dB to 10 dB, justified by the fact that the majority of measured values given in [16] are within this range for urban, suburban and rural areas. Observing the values of μ_K and σ_K given in Section II, it can be concluded that they have a negative correlation, which can be justified by the fact that lower values of μ_K correspond to areas with high density and a variety of obstacles between the PU transmitter and the SUs, thus yielding a higher σ_K. On the other hand, higher values of μ_K correspond to areas with small influence of obstacles, leading to lower values of σ_K.

Fig. 2 shows a linear regression result applied to the measurements reported in [16], from where the value of σ_K for a given μ_K was retrieved and used in the computer simulations. Specifically, for $\mu_K = [-10, -7.5, -5, -2.5, 0, 2.5, 5, 7.5, 10]$ dB, which were the values adopted hereafter, it follows that $\sigma_K = [9.32, 8.23, 7.13, 6.04, 4.94, 3.85, 2.75, 1.66, 0.56]$ dB. Unless otherwise specified, the remaining parameters are: number of SUs $m = 6$, SNR $= -12$ dB, path loss exponent

$\eta = 2$, coverage radius $r = 1$ km, reference distance $d_0 = 1$ m, PU transmit power $P_{\text{tx}} = 5$ W, PU transmitter located at $(1, 1)$ km, number of samples $n = 250$, fraction of noise variation $\rho = 0.5$, constant false alarm rate $P_{\text{fa}} = 0.1$.

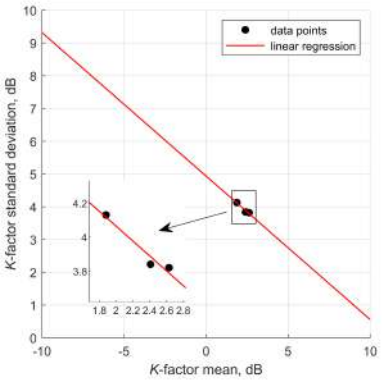

Fig. 2: Linear regression applied to the pairs of Rice K-factor means and corresponding standard deviations reported in [16].

Each figure presented hereafter gives the probability of detection, P_{d}, as a function of the mean Rice factor, μ_K, for two values of other important system parameters. Each point on a curve has been generated from 20000 Monte Carlo simulation runs, which corresponds to the same amount of spectrum sensing events. The MATLAB code used to obtain the results is available at [21].

Fig. 3 shows P_{d} versus μ_K for two values of the path loss exponent, $\eta = 2$ and $\eta = 4$. It can be seen that the detectors GID and PRIDe are quite sensitive to the Rice factor, with the former being more sensitive than the latter. It can be seen that both are by far more suitable to channels with higher Rice factors than the other detectors. The sensitivities of the detectors GRCR, HR, VD1 and LMPIT to the variation of the Rice factor are quite small, and the detectors GLRT, MMED and AGM attained poor performances for any value of μ_K, which is credited to their high sensitivity to the variation of the noise levels, in this case represented by $\rho = 0.5$. Most of the detectors had their performances reduced from $\eta = 2$ to $\eta = 4$, which is caused by larger discrepancies in the SNR at the SUs when η is larger (recall that the SNR is fixed, meaning that larger values of η yield lower values of the noise powers, on average, to compensate for the lower average received signal powers). The performance penalty caused to the detectors GLRT, MMED and AGM is barely noticed due to the fact that they are already very close to the worst situation, i.e., $P_{\text{d}} \approx P_{\text{fa}} = 0.1$.

Fig. 4 shows P_{d} versus μ_K for two values of the noise level variation fraction, $\rho = 0$ and $\rho = 0.9$. In terms of the influence of the Rice factor, it can be seen a situation similar to the one observed in Fig. 3. Once again, the GID and PRIDe unveil to be more suitable to higher Rice factors. A performance penalty can be observed in all detectors due to the increase of ρ from 0 to 0.9. The penalty is smaller in the case of the GRCR, GID, PRIDe, HR, VD1 and LMPIT, whereas a drastic performance loss is observed in the case of the GLRT, MMED and AGM. In other terms, it can be said that the detectors GLRT, MMED and AGM are significantly less robust to variations in the noise levels the the other ones.

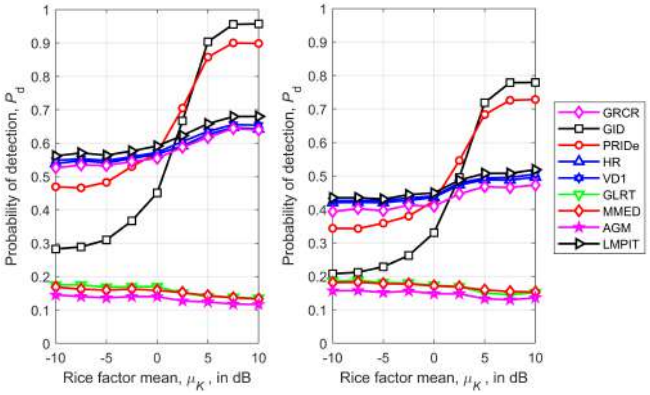

(a) $\eta = 2$ (b) $\eta = 4$

Fig. 3: Probability of detection versus mean Rice factor, for two different values of the path loss exponent.

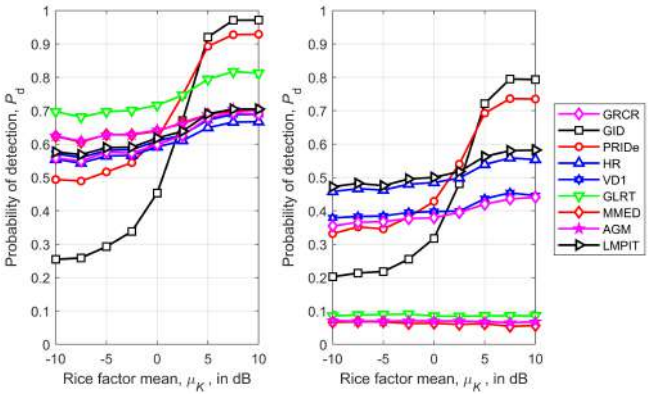

(a) $\rho = 0$ (b) $\rho = 0.9$

Fig. 4: Probability of detection versus mean Rice factor, for two different values of the fraction of noise level variation around the mean.

Fig. 5 shows P_{d} versus μ_K for two different positions of the PU transmitter, namely $(0, 0)$ and $(10, 10)$ km. Once again, it can be seen a situation similar to the one observed in Fig. 3 and Fig. 4, in terms of the influence of the Rice factor, with the GID and PRIDe unveiling to be more suitable to higher values of the Rice factor. Except for the detectors GLRT, MMED and AGM, whose performances are close to the worst case scenario ($P_{\text{d}} \approx P_{\text{fa}} = 0.1$), it can be seen that better performances are achieved when the PU transmitted is located farther apart from the SUs. Again, it must be emphasized that the average SNR is the same for both Fig. 5a and Fig. 5b. Hence, larger distances of the PU transmitter yield smaller differences in the received signal levels at the SUs, which renders higher cooperation gains to the spectrum sensing process.

Finally, the influences of m, n and SNR on P_{d} have not been added to this paper due to length restrictions but also because it is well known that an increase in any of these parameters produce performance improvement for all detectors. In the case of m, it is also known that the performance improvement follows a diminishing-return law; for instance, the performance improvement when m changes from 4 to 8

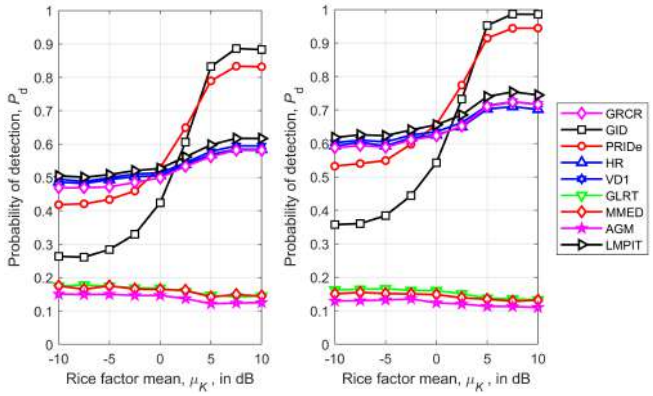

(a) PU Tx at $(0, 0)$ km (b) PU Tx at $(10, 10)$ km

Fig. 5: Probability of detection versus mean Rice factor, for two different locations of the PU transmitter.

is larger than when it goes from 8 to 16.

V. Conclusions

This paper examined the impact of the Rice factor on the performance of state-of-the-art blind detectors for cooperative spectrum sensing. Other realistic scenarios have been also taken into account, like distance-dependent received signal powers, nonuniform receiver noise, and a consistent signal-to-noise ratio calibration procedure. The findings reveal significant effects of the Rice factor on certain detectors, with some of them showing resilience to Rice factor fluctuations. Specifically, it has been shown that the detectors GID and PRIDe are the ones that are more sensitive to variations in the Rice factor, with the former being more sensitive than the latter. Nonetheless, these detectors have unveiled excellent performance in situations of high Rice factor. The detectors GRCR, HR, VD1 and LMPIT have attained relatively low sensitivity to variations in the Rice factor, outperforming the GID and PRIDe at low Rice factor regimes, but being outperformed by the GID and PRIDe when the Rice factor is above 0 dB, approximately. Although the detectors GLRT, MMED and AGM demonstrated to have robustness against Rice factor variations, useful performances were achieved only in the unrealistic situation of uniform noise levels at the receivers. This is because these detectors are known to exhibit low robustness against variations in these noise levels.

Last, but not least, it must be emphasized that the choice of the detector should be guided not only by its performance, but also by its implementation complexity. In this case, deserve attention the detectors GRCR, GID, PRIDe and LMPIT, whose test statistics are formed directly from the elements of the received signal sample covariance matrix. Among these detectors, the PRIDe is highlighted due to outstanding performance at higher Rice factors, and good performance at lower values of this parameter. Recently, a modified version of the PRIDe detector, named mPRIDe [20], has been devised for FPGA (field programmable gate array) and ASIC (application-specific integrated circuit) designs, attaining performance metrics identical to the PRIDe, but having reduced computational complexity, latency and chip area with respect to state-of-the-art solutions reported to date.

References

[1] D. Das and S. Das, "A survey on spectrum occupancy measurement for cognitive radio," *Wirel. Pers. Commun.*, vol. 85, no. 4, p. 2581–2598, Dec 2015, doi: 10.1007/s11277-015-2921-1.

[2] Y. Arjoune and N. Kaabouch, "A comprehensive survey on spectrum sensing in cognitive radio networks: Recent advances, new challenges, and future research directions," *Sensors*, vol. 19, no. 1, 2019, doi: 10.3390/s19010126.

[3] A. Nasser, H. Al Haj Hassan, J. Abou Chaaya, A. Mansour, and K.-C. Yao, "Spectrum sensing for cognitive radio: Recent advances and future challenge," *Sensors*, vol. 21, no. 7, 2021. [Online]. Available: https://www.mdpi.com/1424-8220/21/7/2408

[4] J. Mitola III and G. Q. Maguire Jr., "Cognitive radio: making software radios more personal," *IEEE Personal Commun. Mag.*, vol. 6, no. 4, pp. 13–18, Aug 1999.

[5] Y. Zeng, Y.-C. Liang, A. Hoang, and R. Zhang, "A review on spectrum sensing for cognitive radio: Challenges and solutions," *EURASIP Journal on Advances in Signal Processing*, vol. 2010, no. 1, p. 381465, 2010, doi: 10.1155/2010/381465.

[6] I. F. Akyildiz, B. F. Lo, and R. Balakrishnan, "Cooperative spectrum sensing in cognitive radio networks: A survey," *Elsevier Physical Comm.*, vol. 4, pp. 40–62, mar 2011, doi: 10.1016/j.phycom.2010.12.003.

[7] D. A. Guimarães, "Spectrum sensing: A tutorial," *Journal of Communication and Information Systems*, vol. 37, no. 1, pp. 10–29, Feb. 2022. [Online]. Available: https://jcis.sbrt.org.br/jcis/article/view/811

[8] ——, "Robust test statistic for cooperative spectrum sensing based on the Gerschgorin circle theorem," *IEEE Access*, vol. 6, pp. 2445–2456, 2018, doi: 10.1109/ACCESS.2017.2783443.

[9] ——, "Gini index inspired robust detector for spectrum sensing over Ricean channels," *Electronics Letters*, November 2018, doi: 10.1049/el.2018.7375.

[10] ——, "Pietra-Ricci index detector for centralized data fusion cooperative spectrum sensing," *IEEE Trans. Veh. Technol.*, vol. 69, no. 10, pp. 12 354–12 358, 2020, doi: 10.1109/TVT.2020.3009440.

[11] L. Huang, Y. Xiao, H. C. So, and J. Fang, "Accurate performance analysis of Hadamard ratio test for robust spectrum sensing," *IEEE Trans. Wirel. Commun.*, vol. 14, no. 2, pp. 750–758, Feb 2015.

[12] L. Huang, C. Qian, Y. Xiao, and Q. T. Zhang, "Performance analysis of volume-based spectrum sensing for cognitive radio," *IEEE Trans. Wirel. Commun.*, vol. 14, no. 1, pp. 317–330, Jan 2015.

[13] B. Nadler, F. Penna, and R. Garello, "Performance of eigenvalue-based signal detectors with known and unknown noise level," in *IEEE Int. Conf. Commun.*, Jun 2011, pp. 1–5.

[14] R. Zhang, T. J. Lim, Y. C. Liang, and Y. Zeng, "Multi-antenna based spectrum sensing for cognitive radios: A GLRT approach," *IEEE Trans. Commun.*, vol. 58, no. 1, pp. 84–88, Jan 2010.

[15] D. Ramirez, J. Via, I. Santamaria, and L. L. Scharf, "Locally most powerful invariant tests for correlation and sphericity of Gaussian vectors," *IEEE Trans. Inf. Theory*, vol. 59, no. 4, pp. 2128–2141, April 2013, doi: 10.1109/TIT.2012.2232705.

[16] S. Zhu, T. S. Ghazaany, S. M. R. Jones, R. A. Abd-Alhameed, J. M. Noras, T. Van Buren, J. Wilson, T. Suggett, and S. Marker, "Probability distribution of Rician K-factor in urban, suburban and rural areas using real-world captured data," *IEEE Trans. Antennas Propag.*, vol. 62, no. 7, pp. 3835–3839, Jul 2014, doi: 10.1109/TAP.2014.2318072.

[17] D. A. Guimarães, "Modified Gini index detector for cooperative spectrum sensing over line-of-sight channels," *Sensors*, vol. 23, no. 12, 2023. [Online]. Available: https://www.mdpi.com/1424-8220/23/12/5403

[18] D. A. Guimarães, "Hybrid fusion of Pietra-Ricci index detector information for cooperative spectrum sensing," *Ad Hoc Networks*, vol. 150, p. 103265, 2023. [Online]. Available: https://www.sciencedirect.com/science/article/pii/S1570870523001853

[19] T. S. Rappaport, *Wireless Communications: Principles And Practice*, 2nd ed. Pearson Education, 2010.

[20] D. A. Guimarães, E. J. T. Pereira, and R. Shrestha, "Resource-efficient low-latency modified Pietra-Ricci index detector for spectrum sensing in cognitive radio networks," *IEEE Trans. Veh. Technol.*, pp. 1–15, 2023, doi: 10.1109/TVT.2023.3269345.

[21] D. A. Guimarães, "MATLAB code to simulate the performance of detectors for centralized data fusion cooperative spectrum sensing," Apr 2024. [Online]. Available: https://www.dropbox.com/scl/fi/7semvrun0blm5fm4eomgy/Pd_vs_Rice_Factor.m?rlkey=8znwc9m0r8tirkw54lkr0a8kl&dl=0